DOI: 10.1111/mice.12577

ORIGINAL ARTICLE

A DYNAMICALLY BI-ORTHOGONAL SOLUTION METHOD FOR A STOCHASTIC LIGHTHILL-WHITHAM-RICHARDS TRAFFIC-FLOW MODEL

Tianxiang Fan[1] | S.C. Wong[1,2] | Zhiwen Zhang[3] | Jie Du[4,5]

[1] Department of Civil Engineering, The University of Hong Kong, Hong Kong SAR, China

[2] Guangdong - Hong Kong - Macau Joint Laboratory for Smart Cities

[3] Department of Mathematics, The University of Hong Kong, Hong Kong SAR, China

[4] Yau Mathematical Sciences Center, Tsinghua University, China

[5] Yanqi Lake Beijing Institute of Mathematical Sciences and Applications, Beijing 101408, P.R. China

Correspondence
S.C. Wong, Department of Civil Engineering, The University of Hong Kong, Hong Kong SAR, China
Email: hhecwsc@hku.hk

Funding information
Research Grants Council (RGC) of the Hong Kong Special Administrative Region, China (Project No. R5029-18) and the Guangdong-Hong Kong-Macau Joint Laboratory Program of the 2020 Guangdong New Innovative Strategic Research Fund, Guangdong Science and Technology Department (Project No. 2020B1212030009).

ABSTRACT

Macroscopic traffic flow modeling is essential for describing and forecasting the characteristics of traffic flow. However, the classic Lighthill-Whitham-Richards (LWR) model only provides equilibrium values for steady-state conditions and fails to capture stochastic variabilities, which are commonly observed and necessary for accurate modeling of real-time traffic management and control. In this paper, a stochastic LWR (SLWR) model that randomizes free-flow speed is developed to account for the uncertainties incurred by driving behavior. The SLWR model follows a conservation law of stochastic traffic density and flow and is formulated as a time-dependent stochastic partial differential equation. The model is solved by a dynamically bi-orthogonal (DyBO) method based on spatial and stochastic bases. Various scenarios are simulated and compared to the Monte Carlo method, and the results show that the SLWR model can effectively describe dynamic traffic evolutions and that the DyBO method shows significant computational advantages over the Monte Carlo method.

1 INTRODUCTION

Traffic flow modeling is fundamental for describing and predicting the characteristics of vehicular movements, and it is an important component of dynamic traffic assignment and real-time traffic management and control. At the macroscopic level, traffic flow modeling focuses on the dynamic changes in flow, density, and speed, as well as shock formation and propagation, with the Lighthill-Whitham-Richards (LWR) model (Lighthill and Whitham, 1955; Richards, 1956) being a classic and popular model. The LWR model is a time-dependent deterministic partial differential equation that obeys a conservation law of traffic density and flow. However, it ignores stochastic variabilities, which are common because of differences in driving behavior, vehicle types, and road conditions. The LWR model must be extended to capture these stochastic variabilities in traffic

flow. However, stochastic modeling increases the computational burden, so an efficient solution method should be developed to improve its applicability in engineering practice.

Stochastic phenomena are commonly observed in daily traffic (Sumalee et al., 2011a; Szeto et al., 2011; Zhou et al., 2016). For example, the space-mean speed can change in response to a change in mean density. Therefore, it is unrealistic to assume that a density evolution pattern is consistent across days, even at the same location, with the same traffic demands. The average travel time may fluctuate within a range at the same period from day to day. Because the classic LWR model describes traffic dynamics as temporal means (Prigogine and Herman, 1971), considerable effort has been made to explore stochastic traffic flow modeling. Exploring how stochasticity can affect the traffic flow, Sumalee et al. (2011) pointed out that randomness can come from exogenous sources such as traffic, road geometry design features, and weather conditions, or from endogenous sources such as driving. Previous studies have suggested three strategies to consider these uncertainties. One is to randomize the density function. Sumalee et al. (2011) proposed a stochastic cell transmission model with a zero-mean Gaussian random process to form the probabilistic density. Randomizing the speed function can also be effective. Li et al. (2012) modified the speed-density function by including a random noise term and then developed an extended LWR model based on these random fundamental relationships. Another option is to randomize the flow function. Jabari and Liu (2012) developed a cell transmission model (CTM)- based stochastic model using random state-dependent vehicle time headways. They also argued that adding random noise terms to a deterministic equation can lead to problems with negative densities and mean dynamics that are inconsistent with those in the deterministic dynamics, which was a common way to model stochastic traffic flow (Gazis and Liu, 2003; Gazis and Knapp, 1971). In their research, traffic dynamics can randomly change at any time step. However, it is unrealistic to expect random changes in driving behavior on the roads. To address this drawback of the unreasonable physical meaning of the stochastic process, this paper assumed that stochasticity stemmed from driving behavior and that once a vehicle entered a road section, its free-flow speed should remain constant. Therefore, a random free-flow speed was introduced into the LWR model and a stochastic partial differential equation (SPDE) was constructed.

Although much research has been done to solve SPDEs, it is challenging to balance accuracy and efficiency. The Monte Carlo (MC) method is a classic and robust way to calculate stochastic solutions, and one of its desirable features is that the convergence rate is independent of stochastic dimensionality (Cheng et al., 2013a). However, a disadvantage of the MC method is its slow convergence. Researchers have studied more efficient solution methods such as the sparse grid-based stochastic collocation method (Babuška et al., 2007), the multi-level Monte Carlo method (Giles, 2008), and the internal Monte Carlo method (Jahani et al., 2014). Jahani et al. (2014) modeled uncertain variables as fuzzy random variables and evaluated them by interval Monte Carlo simulation and the interval finite element method. These methods can be categorized as sampling techniques. Furthermore, generalized polynomial chaos (Xiu et al., 2002) and multi-element generalized polynomial chaos (Wan and Karniadakis, 2006) are spectral methods for solving uncertainty problems. Another approach is to formulate a reduced-complexity model that retains as much of the original predictive capability as possible, such as the Karhunen-Loeve (KL) expansion or the Wiener-Askey polynomial chaos expansion. Newman (1996a, 1996b) showed how to use the Karhunen-Loeve expansion and Galerkin's method to find reduced-complexity models for flow-involved dynamical systems. Xiu and Karniadakis (2003) proposed a Wiener-Askey polynomial chaos expansion to represent stochastic processes and demonstrated an exponential convergence rate by solving a stochastic ordinary differential equation. However, these methods require the formation of covariance matrices and the solving of large-scale eigenvalue problems, both of which are computationally expensive. To solve this problem, researchers have studied a dynamically bi-orthogonal (DyBO) method (Babaee et al., 2017; Cheng et al., 2013a, 2013b; Choi et al., 2014) that derives an equivalent system governing the evolution of the spatial and stochastic bases in the KL expansion. This method constructed a reduced basis on the fly without the need to form the covariance matrix or compute its eigendecomposition. Such a method is rarely used in stochastic traffic flow modeling, so it is interesting to examine its applicability.

To capture the stochastic traffic characteristics, a Stochastic Lighthill-Whitman-Richards (SLWR) model in which the free-flow speed was randomized to account for driving behavior, was developed. In addition, in various simulation experiments, the DyBO method was used to efficiently obtain numerical solutions compared with the results of the MC method.

2 STOCHASTIC TRAFFIC FLOW MODEL

In macroscopic modeling, traffic flow is described as a continuous fluid, and the distribution, evolution, and propagation of density, speed, and flow are studied. A homogeneous highway with a uniform road configuration is assumed, where all vehicles enter the road section at the entrance and travel to the exit without any entries or exits along the road (see Figure 1).

The traffic flow at the entrance consists of various drivers, each with a different desired speed in free-flow traffic. For example, conservative drivers travel more slowly than aggressive drivers. This heterogeneous driving behavior may result in stochastic phenomena. Therefore, some assumptions are made before the SLWR model is developed.

- *Different drivers have different driving behaviors (represented by the free-flow speed, which is assumed to follow a certain distribution).*
- *Vehicle compositions at the road entrance are randomly affected by the distribution of the free-flow speed, and once a vehicle enters the road, its driving behavior should remain constant until it exits.*

Let u_f be the free-flow speed, which is a random variable that could follow any type of distribution, defined on a probability space $(\Omega, \mathcal{F}, \mathbb{P})$, representing heterogeneous driving behavior,

$$u_f: \Omega \to \mathbb{R}, \tag{1}$$

where Ω is a sample space, $\mathcal{F}$ is a σ-algebra, $\mathbb{P}$ is a probability measure and $\mathbb{R}$ is a real line. Then, $u_f(\omega)$ is the random free-flow speed that corresponds to the random event $\omega \in \Omega$.

At the entrance, traffic flow is a stochastic process defined on the same probability space,

$$\{Q_{in}(t,\omega): t \in [0,T], \omega \in \Omega\}, \tag{2}$$

where $Q_{in}(t,\omega)$ is the traffic flow at the entrance and t represents the evolving time from 0 to T. Therefore, every $t \in [0,T]$ corresponds to some random variable $Q_{in}(t,\cdot): \Omega \to \mathbb{R}$, which indicates that traffic flow at the entrance can randomly change over time.

In combination with the definitional relationship and the Greenshield's model, the traffic dynamics of any certain driver can be described by

$$q\big(x,t,u_f(\omega)\big) = k\big(x,t,u_f(\omega)\big)u\big(x,t,u_f(\omega)\big), \tag{3}$$

$$u\left(x,t,u_f(\omega)\right) = u_f(\omega) - \frac{u_f(\omega)}{k_{jam}} k\left(x,t,u_f(\omega)\right), \tag{4}$$

where $q\big(x,t,u_f(\omega)\big)$ is the traffic flow, $k\big(x,t,u_f(\omega)\big)$ is the traffic density, $u\big(x,t,u_f(\omega)\big)$ is the traffic speed, and k_{jam} is the jam density. These show that for a given free-flow speed, traffic dynamics are non-random variables across the highway section over time.

In light of fluid mechanics, vehicular movements through the assumed homogeneous highway section can be described in terms of the conservation law, so general specification of the SLWR model can be described as follows:

$$\frac{\partial k(x,t,u_f(\omega))}{\partial t} + \frac{\partial q(x,t,u_f(\omega))}{\partial x} = 0,\ x \in [a,b], t \in [0,T], \omega \in \Omega, \tag{5}$$

$$k\big(x,0,u_f(\omega)\big) = k_0\left(x,u_f(\omega)\right), \tag{6}$$

$$q\big(a,t,u_f(\omega)\big) = Q_{in}(t,\omega), \tag{7}$$

where x represents the spatial dimension, i.e., the length of the road section from point a to point b; Equation (5) is the conservation law, Equation (6) shows the initial condition, and Equation (7) shows the boundary condition.

The proposed model indicates that the boundary condition will evolve randomly, but once the free-flow speed is sampled, its corresponding traffic dynamics will obey the conservation law. This means that randomness only enters the system through the boundary condition because of heterogeneous driving behavior, which satisfies our assumptions.

3 SOLUTION METHODS

To numerically solve the SLWR model, the DyBO method was first adopted to transform the SPDE into a series of deterministic partial differential equations (PDE) and ordinary differential equations (ODE). Classic finite difference methods can then be applied. The fifth-order weighted essentially non-oscillatory (WENO5) scheme was used.

3.1 Dynamically bi-orthogonal solution method

The derivation of the DyBO formulation of the SLWR model is presented below. Combining Equations (3), (4), and (5), the SLWR model can be written as

$$\frac{\partial k\left(x,t,u_f(\omega)\right)}{\partial t} = \mathcal{L}k = \left(2\frac{u_f(\omega)}{k_{jam}} k\left(x,t,u_f(\omega)\right) - u_f(\omega)\right)\frac{\partial k\left(x,t,u_f(\omega)\right)}{\partial x}, \tag{8}$$

where $\mathcal{L}$ is a differential operator and k_{jam} is the jam density (a constant value).

According to the KL expansion (Newman, 1996a), denote by $\tilde{k}$ the m-term truncated solution of Equation (8),

$$\tilde{k} = \bar{k} + \boldsymbol{k}\boldsymbol{Y}^T, \tag{9}$$

$$\boldsymbol{k}(x,t) = \big(k_1(x,t), k_2(x,t), \dots, k_m(x,t)\big), \tag{10}$$

$$\boldsymbol{Y}(\omega,t) = \big(Y_1(\omega,t), Y_2(\omega,t), \dots, Y_m(\omega,t)\big), \tag{11}$$

$$Cov_k(x,y) = E\left[\left(k\left(x,t,u_f(\omega)\right) - \bar{k}(x,t)\right)\left(k\left(y,t,u_f(\omega)\right) - \bar{k}(y,t)\right)\right], \tag{12}$$

where $\bar{k} = E[\tilde{k}]$, $\boldsymbol{k}(x,t)$ is the spatial basis, i.e., a vector of eigenfunctions of the associated covariance function of Equation (12); $\boldsymbol{Y}(\omega,t)$ is the stochastic basis, i.e., a vector of zero-mean random variables; and m is the number of truncated terms. Correspondingly, $\langle \boldsymbol{k}^T, \boldsymbol{k} \rangle$ and $E[\boldsymbol{Y}^T\boldsymbol{Y}]$ are m-by-m matrices and satisfy the bi-orthogonality condition as

$$\langle \boldsymbol{k}^T, \boldsymbol{k} \rangle(t) = \big(\langle k_i, k_j \rangle\big) = (\lambda_i(t)\delta_{ij})_{m\times m}, \tag{13}$$

$$E[\boldsymbol{Y}^T\boldsymbol{Y}](t) = \big(E[Y_iY_j]\big) = \boldsymbol{I}, \tag{14}$$

where $\lambda_i(t)$ is the corresponding eigenvalues of the covariance function of Equation (12), δ_{ij} is the Kronecker product, and $\boldsymbol{I}$ is the identity matrix.

Substitute Equation (9) into Equation (8),

$$\frac{\partial \bar{k}}{\partial t} + \frac{\partial \boldsymbol{k}}{\partial t}\boldsymbol{Y}^T + \boldsymbol{k}\frac{d\boldsymbol{Y}^T}{dt} = \mathcal{L}\tilde{k} + \{\mathcal{L}k - \mathcal{L}\tilde{k}\} - \left\{\frac{\partial \tilde{\boldsymbol{k}}}{\partial t}\tilde{\boldsymbol{Y}}^T + \tilde{\boldsymbol{k}}\frac{d\tilde{\boldsymbol{Y}}^T}{dt}\right\}, \tag{15}$$

and assume that the eigenvalues in the KL expansion decay fast enough and the differential operator is stable; then, the last two terms on the right-hand side will be small and can be dropped.

$$\frac{\partial \bar{k}}{\partial t} + \frac{\partial \boldsymbol{k}}{\partial t}\boldsymbol{Y}^T + \boldsymbol{k}\frac{d\boldsymbol{Y}^T}{dt} = \mathcal{L}\tilde{k}. \tag{16}$$

Take expectations on both sides of Equation (15), and because $\boldsymbol{Y}$ is a zero-mean random variable,

$$\frac{\partial \bar{k}}{\partial t} = E\left[\mathcal{L}\tilde{k}\right], \tag{17}$$

which gives the evolution equation for the mean of the solution.

Multiplying both sides of Equation (16) by Y from the right and taking expectations, the evolution equation of the spatial basis can be obtained. Similarly, multiplying both sides of Equation (16) by k from the right, the evolution equation of the stochastic basis can be obtained. More detailed steps of the derivation can be found in Cheng et al. (2013).

$$\frac{\partial \boldsymbol{k}}{\partial t} = -\boldsymbol{k}\boldsymbol{D}^T + E\left[\tilde{\mathcal{L}}\tilde{k}\boldsymbol{Y}\right], \tag{18}$$

$$\frac{d\boldsymbol{Y}}{dt} = -\boldsymbol{Y}\boldsymbol{C}^T + \langle\tilde{\mathcal{L}}\tilde{k}, \boldsymbol{k}\rangle\boldsymbol{\Lambda}_{\boldsymbol{k}}^{-1}, \tag{19}$$

where $\boldsymbol{C}$ and $\boldsymbol{D}$ are m-by-m matrices representing the projection coefficients of $\frac{\partial \boldsymbol{k}}{\partial t}$ and $\frac{d\boldsymbol{Y}}{dt}$ into $\boldsymbol{k}$ and $\boldsymbol{Y}$, respectively. The solutions of $\boldsymbol{C}$ and $\boldsymbol{D}$ are given entry-wisely,

$$C_{ii} = G_{*ii}, \tag{20}$$

$$C_{ij} = \frac{\|k_j\|^2}{\|k_j\|^2 - \|k_i\|^2}\left(G_{*ij} + G_{*ji}\right),\ for\ i \neq j, \tag{21}$$

$$D_{ii} = 0, \tag{22}$$

$$D_{ij} = \frac{1}{\|k_j\|^2 - \|k_i\|^2}\left(\|k_j\|^2 G_{*ji} + \|k_i\|^2 G_{*ij}\right),\ for\ i \neq j, \tag{23}$$

where C_{ii}, C_{ij} are elements of the matrix $\boldsymbol{C}$; D_{ii}, D_{ij} are elements of the matrix $\boldsymbol{D}$; and G_{*ij}, G_{*ji} are elements of the matrix $\boldsymbol{G}_*$, which can be calculated as

$$\boldsymbol{G}_* = \boldsymbol{\Lambda}_{\boldsymbol{k}}^{-1}\langle\boldsymbol{k}^T, E\left[\tilde{\mathcal{L}}\tilde{k}\boldsymbol{Y}\right]\rangle, \tag{24}$$

$$\boldsymbol{\Lambda}_{\boldsymbol{k}} = diag(\langle\boldsymbol{k}^T, \boldsymbol{k}\rangle). \tag{25}$$

Equations (18) and (19) still involve random variables. Because the random free-flow speed is assumed to follow a normal distribution in this paper, Hermite polynomials can be used to represent the stochastic terms.

Denote by $\boldsymbol{H} = (H_1, H_2, \cdots, H_{N_p})$ the N_p -term Hermite polynomials, which exclude the zero-index $\boldsymbol{H}_0 = 1$. Then,

$$\boldsymbol{Y} = \boldsymbol{H}\boldsymbol{A}, \tag{26}$$

where $\boldsymbol{A}$ is a N_p-by-m matrix.

Denote by $Z_{u_f} = \boldsymbol{c}\boldsymbol{H}^T$ a standard normal (i.e., $Z_{u_f} \sim N(0,1)$), where $\boldsymbol{c} = (1,0,\cdots,0)$ is the expansion constants; then, the free-flow speed can be represented as

$$u_f(\omega) = \overline{u_f} + \sigma_{u_f}\boldsymbol{c}\boldsymbol{H}^T, \tag{27}$$

where $\overline{u_f}$ is the mean and σ_{u_f} is the standard deviation of the random free-flow speed.

Substituting Equations (9), (26), and (27) into Equation (8),

$$\begin{aligned}\mathcal{L}\tilde{k} = &\left(2\frac{u_f(\omega)}{k_{jam}}\bar{k} - u_f(\omega)\right)\frac{\partial \bar{k}}{\partial x} + \left(\frac{2\bar{k}}{k_{jam}} - 1\right)\overline{u_f}\boldsymbol{H}\boldsymbol{A}\frac{\partial \boldsymbol{k}^T}{\partial x} + \\ &\left(\frac{2\bar{k}}{k_{jam}} - 1\right)\sigma_{u_f}\boldsymbol{c}\boldsymbol{H}^T\boldsymbol{H}\boldsymbol{A}\frac{\partial \boldsymbol{k}^T}{\partial x} + \frac{2}{k_{jam}}\frac{\partial \bar{k}}{\partial x}\overline{u_f}\boldsymbol{H}\boldsymbol{A}\boldsymbol{k}^T + \\ &\frac{2}{k_{jam}}\frac{\partial \bar{k}}{\partial x}\sigma_{u_f}\boldsymbol{c}\boldsymbol{H}^T\boldsymbol{H}\boldsymbol{A}\boldsymbol{k}^T + \frac{2}{k_{jam}}\overline{u_f}\boldsymbol{k}\boldsymbol{A}^T\boldsymbol{H}^T\boldsymbol{H}\boldsymbol{A}\frac{\partial \boldsymbol{k}^T}{\partial x} + \\ &\frac{2}{k_{jam}}\sigma_{u_f}\boldsymbol{c}\boldsymbol{H}^T\boldsymbol{k}\boldsymbol{A}^T\boldsymbol{H}^T\boldsymbol{H}\boldsymbol{A}\frac{\partial \boldsymbol{k}^T}{\partial x}.\end{aligned} \tag{28}$$

Then, the following terms $E\left[\mathcal{L}\tilde{k}\right], E\left[\tilde{\mathcal{L}}\tilde{k}\boldsymbol{H}\right]\boldsymbol{A} = E\left[(\mathcal{L}\tilde{k} - E[\mathcal{L}\tilde{k}])\boldsymbol{H}\right]\boldsymbol{A}, E\left[\boldsymbol{H}^T\tilde{\mathcal{L}}\tilde{k}\right]$ can be calculated using the properties $E[\boldsymbol{H}^T\boldsymbol{H}] = \boldsymbol{I}$, $\boldsymbol{A}^T\boldsymbol{A} = \boldsymbol{I}$, and $E[\boldsymbol{H}] = \boldsymbol{0}$.

Based on the representation of Hermite polynomials, the DyBO formulation of the SLWR model can be expressed as

$$\frac{\partial \bar{k}}{\partial t} = E\left[\mathcal{L}\tilde{k}\right], \tag{29}$$

$$\frac{\partial \boldsymbol{k}}{\partial t} = -\boldsymbol{k}\boldsymbol{D}^T + E\left[\tilde{\mathcal{L}}\tilde{k}\boldsymbol{H}\right]\boldsymbol{A}, \tag{30}$$

$$\frac{d\boldsymbol{A}}{dt} = -\boldsymbol{A}\boldsymbol{C}^T + \langle E\left[\boldsymbol{H}^T\tilde{\mathcal{L}}\tilde{k}\right], \boldsymbol{k}\rangle\boldsymbol{\Lambda}_{\boldsymbol{k}}^{-1}, \tag{31}$$

which gives the deterministic PDE of Equations (29) and (30) and ODE of Equation (31).

3.2 Weighted essentially non-oscillatory scheme

This study used the fifth-order WENO5 scheme. This method has high resolution and is non-oscillatory even in the presence of shocks and other discontinuities in the solution (Xiong et al., 2011). More details can be found in Shu (2006) and Shu (2020). The procedure of the WENO scheme is summarized below. Consider Equation (29) as an example.

First, spatial discretization is discussed. The space domain is discretized into a uniform mesh of J grid points:

$$x_j = j\Delta x, j = 1,2,\cdots,J, \tag{32}$$

where Δx is the uniform grid mesh. Then, the approximation of density $\bar{k}_j(t) \approx \bar{k}(x_j, t)$ satisfies the following equation:

$$\frac{d\bar{k}_j(t)}{dt} + \frac{1}{\Delta x}\left(\hat{q}_{j+\frac{1}{2}} - \hat{q}_{j-\frac{1}{2}}\right) = 0, \tag{33}$$

where $\hat{q}_{j+\frac{1}{2}}$ and $\hat{q}_{j-\frac{1}{2}}$ are the numerical fluxes at points j+1/2 and j-1/2 of the right-hand side of Equation (28), respectively. According to the fifth-order WENO scheme, the numerical flux $\hat{q}_{j+\frac{1}{2}}$ is defined as follows:

$$\hat{q}_{j+\frac{1}{2}} = \theta_1 \hat{q}^{(1)}_{j+1/2} + \theta_2 \hat{q}^{(2)}_{j+1/2} + \theta_3 \hat{q}^{(3)}_{j+1/2}, \quad (34)$$

where θ_1, θ_2, and θ_3 are three nonlinear weights and $\hat{q}^{(1)}_{j+1/2}$, $\hat{q}^{(2)}_{j+1/2}$, and $\hat{q}^{(3)}_{j+1/2}$ are three third-order numerical fluxes on three stencils. The third-order fluxes are given by

$$\hat{q}^{(1)}_{j+1/2} = \frac{1}{3}q_{j-2} - \frac{7}{6}q_{j-1} + \frac{11}{6}q_j, \quad (35)$$

$$\hat{q}^{(2)}_{j+1/2} = -\frac{1}{6}q_{j-1} + \frac{5}{6}q_j + \frac{1}{3}q_{j+1}, \quad (36)$$

$$\hat{q}^{(3)}_{j+1/2} = \frac{1}{3}q_j + \frac{5}{6}q_{j+1} - \frac{1}{6}q_{j+2}, \quad (37)$$

where q_j is an abbreviated notation for $q(x_j, t)$. The nonlinear weights are given by

$$\theta_p = \frac{\tilde{\theta}_p}{\sum_{l=1}^{3}\tilde{\theta}_l}, p = 1,2,3, \quad (38)$$

$$\tilde{\theta}_l = \frac{\gamma_l}{(\varepsilon+\beta_l)^2}, l = 1,2,3, \quad (39)$$

where ε is a parameter to prevent the denominator of $\tilde{\theta}_l$ from being zero and is fixed at 10^{-6} in this paper, γ_l is the linear weights, and β_l is the smoothness indicators. The linear weights are given by

$$\gamma_1 = \frac{1}{10}, \gamma_2 = \frac{3}{5}, \gamma_3 = \frac{3}{10}, \quad (40)$$

and the smoothness indicators are given by

$$\beta_1 = \frac{13}{12}(q_{j-2} - 2q_{j-1} + q_j)^2 + \frac{1}{4}(q_{j-2} - 4q_{j-1} + 3q_j)^2, \quad (41)$$

$$\beta_2 = \frac{13}{12}(q_{j-1} - 2q_j + q_{j+1})^2 + \frac{1}{4}(q_{j-1} - q_{j+1})^2, \quad (42)$$

$$\beta_3 = \frac{13}{12}(q_j - 2q_{j+1} + q_{j+2})^2 + \frac{1}{4}(3q_j - 4q_{j+1} + q_{j+2})^2. \quad (43)$$

Above is described the fifth-order WENO scheme for the positive wind direction. If the wind direction is negative, the procedure for computing the numerical flux $\hat{q}_{j+\frac{1}{2}}$ is a mirror image with respect to the point $x_{j+1/2}$, which is described above. The stencil can then be biased to the right. For the case where the wind direction may change, the Lax-Friedrichs splitting method is used.

$$q(\bar{k}) = q^+(\bar{k}) + q^-(\bar{k}), \quad (44)$$

$$q^{\pm}(\bar{k}) = \frac{1}{2}(q(\bar{k}) \pm \alpha\bar{k}), \quad (45)$$

$$\alpha = max_k\left|\partial q(\bar{k})/\partial\bar{k}\right|, \quad (46)$$

where $q^+(\bar{k})$ and $q^-(\bar{k})$ are the splitting flux for the positive and negative wind directions, respectively.

Second, the time domain is discretized into a mesh of N grid points.

$$t^{[n]} = t^{[n-1]} + \Delta t, n = 1,2,\cdots,N, \quad (47)$$

where Δt is the uniform mesh size on the time axis. Then, the third-order total variation diminishing (TVD) Runge-Kutta method is used.

$$\bar{k}^{(1)} = \bar{k}^{[n]} + \Delta t L(\bar{k}^{[n]}, t^{[n]}), \quad (48)$$

$$\bar{k}^{(2)} = \frac{3}{4}\bar{k}^{[n]} + \frac{1}{4}\bar{k}^{(1)} + \frac{1}{4}\Delta t L(\bar{k}^{(1)}, t^{[n]} + \Delta t), \quad (49)$$

$$\bar{k}^{[n+1]} = \frac{1}{3}\bar{k}^{[n]} + \frac{2}{3}\bar{k}^{(2)} + \frac{2}{3}\Delta t L\left(\bar{k}^{(2)}, t^{[n]} + \frac{1}{2}\Delta t\right), \quad (50)$$

where L is the approximation to the spatial derivatives,

$$L(k,t) = -\frac{1}{\Delta x}\left(\hat{q}_{j+\frac{1}{2}} - \hat{q}_{j-\frac{1}{2}}\right). \quad (51)$$

4 NUMERICAL EXAMPLE

A simulation experiment was conducted to show the effectiveness of the SLWR model. The DyBO method was validated in comparison to the MC method. Different samples of the MC method were calculated to select a benchmark result, and different numbers of spatial terms and Hermite polynomials were tested in the sensitivity analysis.

4.1 Example settings

A 2-km homogeneous road section without any intermediate ramps was considered in the numerical experiment. The free-flow speed was assumed to be a stochastic variable following a normal distribution with a mean of 70 and a standard deviation of 10, i.e., $u_f \sim N(70,100)$ and $k_{jam} = 100\ veh/km$. The initial condition assumed that traffic density was empty along the section, and the boundary condition assumed that traffic flow at the entrance was subjected to a trapezoid of changes, as shown in Figure 2.

It was assumed that an incident can happen at the downstream exit of the road section, blocking the exit from t = 0.75 h to t = 0.77 h. As no vehicles could leave the road section, a queue emerged and propagated upstream. After t = 0.77 h, the incident was cleared, and the queue was able to discharge. For the WENO5 scheme, the spatial and time grid sizes were set to 0.01 km and 1×10-4 h, respectively.

4.2 Numerical results

To validate the DyBO method, a benchmark solution was calculated using the MC method. According to the central limit theorem, as the sample sizes increased, the results of the MC method became closer to the exact values. Samples sizes of 100, 200, 400, 800, 1,600, 3,200, and 12,800 were calculated, and 12,800 samples were computed to approximate the exact solution as a benchmark result. The relative root-mean-squared error (RRMSE) is defined as follows to measure accuracy against the benchmark results.

$$RRMSE_\rho = \frac{\sqrt{\frac{1}{N}\Sigma_{it}\left(\rho_{it}^{(k)} - \rho_{it}^*\right)^2}}{\frac{1}{N}\Sigma_{it}\rho_{it}^*} \times 100\%, \quad (52)$$

$$RRMSE_\sigma = \frac{\sqrt{\frac{1}{N}\Sigma_{it}\left(\sigma_{it}^{(k)} - \sigma_{it}^*\right)^2}}{\frac{1}{N}\Sigma_{it}\sigma_{it}^*} \times 100\%, \quad (53)$$

where $\rho_{it}^{(k)}$ and $\sigma_{it}^{(k)}$ are the mean (MEAN) and standard deviation (SDEV) of the density of the kth case for grid point (i,t), respectively; ρ_{it}^{*} and σ_{it}^{*} are the converged MEAN and SDEV of the density from the MC scheme, respectively; and N is the total number of grid points (space and time).

Figure 3 shows the RRMSE of the MEAN and SDEV of the density. The MEAN's RRMSE converged faster than that of SDEV. When the sample size was larger than 1600, the MEAN's RRMSE dropped below 0.5%, while the SDEV's RRMSE was approximately 3%.

Although the MC method can obtain robust solutions, its efficiency may be undesirable. As shown in Figure 4, the computation time of the MC method increased linearly, and the case of 12,800 samples requires approximately 12,325 min of computing time.

The DyBO method was then applied to reach an acceptable level of accuracy in a much more efficient way. As a blockage incident was considered in the simulation experiment, the results are elaborated in three scenarios: (1) before the blockage, (2) during the blockage, and (3) after the blockage. This can help to clarify the traffic flow propagation. As mentioned, the derivation of DyBO equations involved truncated terms. Therefore, the number of spatial terms or Hermite polynomials can affect the accuracy of the solutions. Different numbers of spatial terms (i.e., $m = 3, 5, 7, 9, 11, 13, 15$) and Hermite polynomials (i.e., $N_p = 2, 4, 6$) were tested to examine the sensitivity of accuracy and efficiency.

Before the blockage, traffic entered at the left boundary and exited at the right boundary without any disturbance, and a relatively smooth density pattern was observed. Figure 5 shows the density patterns at t = 0.3 h. Slight staircase-shaped fluctuations were observed, as vehicles with different free-flow speeds entered stochastically, and faster vehicles traveled farther than slower ones, causing the density to accumulate at different spots. The greater the speed differences, the greater the fluctuations, in line with the findings of Zhang et al. (2003). Furthermore, with increasing spatial terms and Hermite polynomials, the MEAN and SDEV became closer to the results of the MC method.

During the blockage, traffic continuously entered at the left boundary but did not leave at the right boundary. A backward shock wave was observed. Figure 6 shows the density patterns at t = 0.78 h. The maximum MEAN was 100 veh/h, which is consistent with the jam density of the proposed Greenshield's model. The MEAN dropped to approximately 50 veh/h after the peak, indicating the saturated discharging flow, which is consistent with the optimal density of the Greenshield's model. In light traffic, the SDEV was smaller and stable; in congested traffic, the SDEV was larger and unstable; from congested to discharging traffic, the SDEV was smaller and more stable. The queue lengths (i.e., stop-and-go condition) of different groups of drivers can vary greatly, but the middle parts of the queues (i.e., completely stopped condition) are nearly at the same place. According to the fundamental diagram, shockwave speeds decrease as densities increase in the free flow condition, whereas shockwave speeds increase as densities increase in the oversaturated condition. Therefore, with more heterogeneous drivers, the SDEV becomes larger. Even with the shock wave, the DyBO method showed good convergence to the MC results, and the accuracy can be increased by adding more spatial terms and Hermite polynomials.

After the blockage, the queue was discharged at the right boundary, and similar density patterns to those observed before the blockage were observed. Figure 7 shows the density patterns at t = 1.2 h. The MEAN and SDEV were relatively stable alongside the road section, with slight fluctuations because of heterogeneous driving behavior, and were generally larger than those at t = 0.3 h because of the increased traffic flow at the left boundary. This implies that the SLWR model and DyBO method can adapt well to different boundary conditions.

To quantify the convergence of the DyBO method, the RRMSE of MEAN and SDEV were calculated, with different numbers of spatial terms ($m = 3, 5, 7, 9, 11, 13, 15$) and Hermite polynomials ($N_p = 2, 4, 6$) with respect to the benchmark solutions obtained by the MC method with 12,800 samples, as shown in Table 1. As the number of spatial terms or Hermite polynomials increased, the RRMSE of MEAN and SDEV decreased, indicating convergence to the benchmark results. With $m = 15$, the RRMSE of both MEAN and SDEV were below 1%, which was acceptable in comparison to the MC results. Furthermore, the computation time of the DyBO method ranged from 1.7 min to 2.1 min, which considerably reduced the computational costs.

5 DISCUSSION

One major contribution of this paper is the development of an efficient method to solve the SLWR model. The simulation experiment results showed that the DyBO method was much more efficient than the MC method and had desirable accuracy. The speedup performance of the DyBO method was also calculated. It is well known that the convergence of the MC method satisfies the relationship $E = O\left(1/\sqrt{K}\right) = C/\sqrt{K}$, where E is the error, K is the number of MC samples, and C is a constant. Taking the logarithm on both sides, a linear relationship is expected, $lnE = lnC - 1/2\ lnK$. Thus, if a graph of lnE against lnK is plotted, the slope of the best-fitted line can be approximately -0.5. According to the RRMSE and sample size of the MC method in Figure 3, two best-fitted lines were plotted, as shown in Figure 8, from which the number of samples that achieve the same accuracy as the DyBO method can be estimated, and then the speedup can be calculated.

For example, with $m = 15$ and $N_p = 6$, the RRMSE values of MEAN and SDEV were 0.2% and 0.9%, respectively. Based on the best-fitted lines in Figure 8, estimated sample sizes (10,999 and 11,429) can be calculated. To ensure that the accuracy of the DyBO method

was not worse than the MC method in terms of both MEAN and SDEV, the smaller sample size of 10,586 was selected, which took approximately 10,586 min using the MC method. The speedup was then calculated as $10586/2.08 \approx 5089$. As calculated, the DyBO method can achieve approximately 5 to 6000 times speedup over the MC method. As shown in Figure 9, the logarithm of speedup against RRMSE was presented and it was found that the speedup increased as the RRMSE decreased. With respect to the same RRMSE, the speedup of SDEV was greater than that of MEAN, and with respect to the same speedup, the RRMSE of MEAN was less than that of SDEV. For practical use in engineering problems, the balance between efficiency and accuracy can be assessed. If MEAN is more important and a large error can be tolerated, the MC method will remain popular because of its simplicity; however, if SDEV is of interest and sufficiently small errors are desired, then the DyBO method will be preferable.

6 CONCLUSION

This paper developed an SLWR model by introducing a random variable of free-flow speed to account for uncertainties in driving behavior. During the numerical experiments, stochastic variabilities were observed across the roadway section over time, and the MEAN and SDEV of traffic dynamics were then calculated. Compared to the classic LWR model, the proposed model can help to explore the stochastic paradigm, which may be useful in traffic planning, design, and real-time management. For example, if the stochastic speed paradigm is known, it will be feasible to use variable speed limit signs to actively manage real-time traffic operations. Furthermore, a DyBO method was applied to improve the efficiency of solving such stochastic problems, and a sensitivity analysis of the DyBO method was conducted under various settings. In comparison to the MC method, the DyBO method can significantly decrease computation time while maintaining desirable accuracy, thereby increasing its applicability in engineering practice. For example, when addressing road network design problems, the evaluation model must be updated every time network conditions change. It would be very computationally expensive to consider stochasticity in the evaluation model. In such case, the DyBO method can substantially decrease computational burdens. In practice, there are many sources of stochasticity. Future research could consider various vehicle types and traffic stream models.

ACKNOWLEDGMENT

This work was supported by the Research Grants Council (RGC) of the Hong Kong Special Administrative Region, China (Project No. R5029-18) and the Guangdong-Hong Kong-Macau Joint Laboratory Program of the 2020 Guangdong New Innovative Strategic Research Fund, Guangdong Science and Technology Department (Project No. 2020B1212030009). In addition, the first author was supported by a Postgraduate Scholarship from the University of Hong Kong. The second author was supported by the Hong Kong RGC grant project 17204919 and the Francis S Y Bong Professorship in Engineering. The third author was supported by the Hong Kong RGC grant projects (Grant Nos. 17300318 and 17307921). The fourth author was supported by the National Natural Science Foundation of China under Grant Number NSFC 11801302 and the Tsinghua University Initiative Scientific Research Program.

REFERENCES

Babaee, H., Choi, M., Sapsis, T.P. and Karniadakis, G.E. (2017), "A robust bi-orthogonal/dynamically-orthogonal method using the covariance pseudo-inverse with application to stochastic flow problems", Journal of Computational Physics, Vol. 344, pp. 303–319.

Babuška, I., Nobile, F. and Tempone, R. (2007), "A stochastic collocation method for elliptic partial differential equations with random input data", SIAM Journal on Numerical Analysis, Vol. 45 No. 3, pp. 1005–1034.

Cheng, M., Hou, T.Y. and Zhang, Z. (2013a), "A dynamically bi-orthogonal method for time-dependent stochastic partial differential equations I: Derivation and algorithms", Journal of Computational Physics, Vol. 242, pp. 843–868.

Cheng, M., Hou, T.Y. and Zhang, Z. (2013b), "A dynamically bi-orthogonal method for time-dependent stochastic partial differential equations II: Adaptivity and generalizations", Journal of Computational Physics, Vol. 242, pp. 753–776.

Choi, M., Sapsis, T.P. and Em, G. (2014), "On the equivalence of dynamically orthogonal and bi-orthogonal methods: Theory and numerical simulations", Journal of Computational Physics, Vol. 270, pp. 1–20.

Gazis, D. and Liu, C. (2003), "Kalman filtering estimation of traffic counts for two network links in tandem", Transportation Research. Part B: Methodological, Vol. 37 No. 8, pp. 737–745.

Gazis, D.C. and Knapp, C.H. (1971), "On-line estimation of traffic densities from time-series of flow and speed data", Transportation Science, Vol. 5 No. 3, pp. 283–301.

Giles, M.B. (2008), "Multilevel Monte Carlo path simulation", Operations Research, Vol. 56 No. 3, pp. 607–617.

Jabari, S.E. and Liu, H.X. (2012), "A stochastic model of traffic flow: Theoretical foundations", Transportation Research Part B: Methodological, Vol. 46 No. 1, pp. 156–174.

Jahani, E., Muhanna, R.L., Shayanfar, M.A. and Barkhordari, M.A. (2014), "Reliability assessment with fuzzy random variables using interval Monte Carlo simulation", Computer-Aided Civil and Infrastructure Engineering, Vol. 29 No. 3, pp. 208–220.

Li, J., Chen, Q.-Y., Wang, H. and Ni, D. (2012), "Analysis of LWR model with fundamental diagram subject to uncertainties", Transportmetrica, Vol. 8 No. 6, pp. 387–405.

Lighthill, M.J. and Whitham, G.B. (1955), "On kinematic waves. II. A theory of traffic flow on long crowded roads", Proceedings of the Royal Society of London. Series A, Mathematical and Physical Sciences, Vol. 229 No. 1178, pp. 317–345.

Newman, A.J. (1996a), "Model Reduction via the Karhunen-Loeve Expansion Part I: An Exposition", Technical Report T.R.96-32, Institute for Systems Research, University of Maryland, Maryland.

Newman, A.J. (1996b), "Model Reduction via the Karhunen-Loeve Expansion Part II: Some Elementary Examples 1 Introduction", Technical Report T.R.96-32, Institute for Systems Research, University of Maryland, Maryland.

Prigogine, I. and Herman, R. (1971), Kinetic Theory of Vehicular Traffic, Elsevier, New York.

Richards, P.I. (1956), "Shock waves on the highway", Operations Research, Vol. 4 No. 1, pp. 42–51.

Shu, C.-W. (2006), "Essentially non-oscillatory and weighted essentially non-oscillatory schemes for hyperbolic conservation laws", Advanced Numerical Approximation of Nonlinear Hyperbolic Equations, Springer Berlin Heidelberg, Berlin, Heidelberg, pp. 325–432.

Shu, C.W. (2020), "Essentially non-oscillatory and weighted essentially non-oscillatory schemes", Acta Numerica, Vol. 29.

Sumalee, A., Zhong, R.X., Pan, T.L. and Szeto, W.Y. (2011a), "Stochastic cell transmission model (SCTM): A stochastic dynamic traffic model for traffic state surveillance and assignment", Transportation Research Part B: Methodological, Vol. 45 No. 3, pp. 507–533.

Sumalee, A., Zhong, R.X., Pan, T.L. and Szeto, W.Y. (2011b), "Stochastic cell transmission model (SCTM): A stochastic dynamic traffic model for traffic state surveillance and assignment", Transportation Research Part B: Methodological, Vol. 45 No. 3, pp. 507–533.

Szeto, W.Y., Jiang, Y. and Sumalee, A. (2011), "A cell-based model for multi-class doubly stochastic dynamic traffic assignment", Computer-Aided Civil and Infrastructure Engineering, Vol. 26 No. 8, pp. 595–611.

Wan, X. and Karniadakis, G.E.M. (2006), "Multi-element generalized polynomial chaos for arbitrary probability measures", SIAM Journal on Scientific Computing, Vol. 28 No. 3, pp. 901–928.

Xiong, T., Zhang, M., Shu, C.W., Wong, S.C. and Zhang, P. (2011), "High-order computational scheme for a dynamic continuum model for bi-directional pedestrian flows", Computer-Aided Civil and Infrastructure Engineering, Vol. 26 No. 4, pp. 298–310.

Xiu, D. and Em Karniadakis, G. (2003), "The Wiener-Askey polynomial chaos for stochastic differential equations", SIAM Journal on Scientific Computing, Vol. 24 No. 2, pp. 619–644.

Xiu, D., Lucor, D., Su, C.-H. and Karniadakis, G.E. (2002), "Stochastic modeling of flow-structure interactions using generalized polynomial chaos", Journal of Fluids Engineering, Vol. 124 No. 1, pp. 51–59.

Zhang, M., Shu, C.W., Wong, G.C.K. and Wong, S.C. (2003), "A weighted essentially non-oscillatory numerical scheme for a multi-class Lighthill-Whitham-Richards traffic flow model", Journal of Computational Physics, Vol. 191 No. 2, pp. 639–659.

Zhou, B., Bliemer, M.C.J., Bell, M.G.H. and He, J. (2016), "Two new methods for solving the path-based stochastic user equilibrium problem", Computer-Aided Civil and Infrastructure Engineering, Vol. 31 No. 2, pp. 100–116.

TABLE 1. RRMSE of statistical quantities computed by the DyBO and MC methods.

No. of spatial basis	No. of Hermite polynomials: $N_p = 2$			No. of Hermite polynomials: $N_p = 4$			No. of Hermite polynomials: $N_p = 6$		
	MEAN	SDEV	Time (min)	MEAN	SDEV	Time (min)	MEAN	SDEV	Time (min)
m = 3	5.1%	24.5%	1.74	4.2%	23.6%	1.77	3.8%	23.0%	1.82
m = 5	2.2%	13.6%	1.79	2.0%	12.7%	1.81	2.0%	12.2%	1.85
m = 7	1.2%	8.0%	1.82	1.1%	7.3%	1.83	1.0%	6.7%	1.89
m = 9	0.7%	4.4%	1.85	0.6%	3.9%	1.85	0.5%	3.5%	1.93
m = 11	0.5%	3.1%	1.87	0.3%	2.4%	1.90	0.3%	2.0%	1.99
m = 13	0.4%	2.4%	1.89	0.2%	1.4%	1.94	0.2%	1.2%	2.03
m = 15	0.2%	1.7%	1.93	0.2%	1.0%	1.96	0.2%	0.9%	2.08

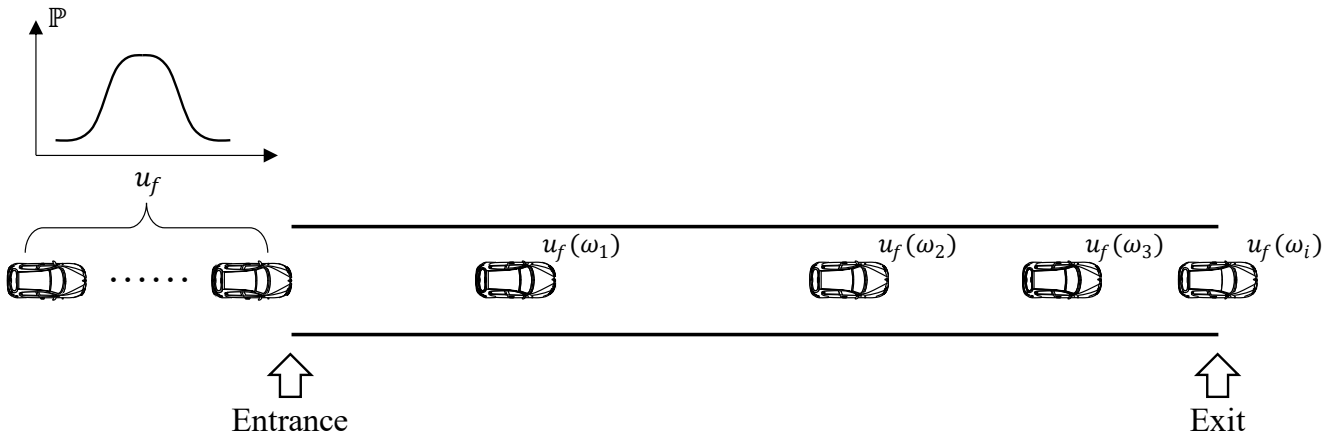

FIGURE 1. Conceptual diagram of the SLWR model.

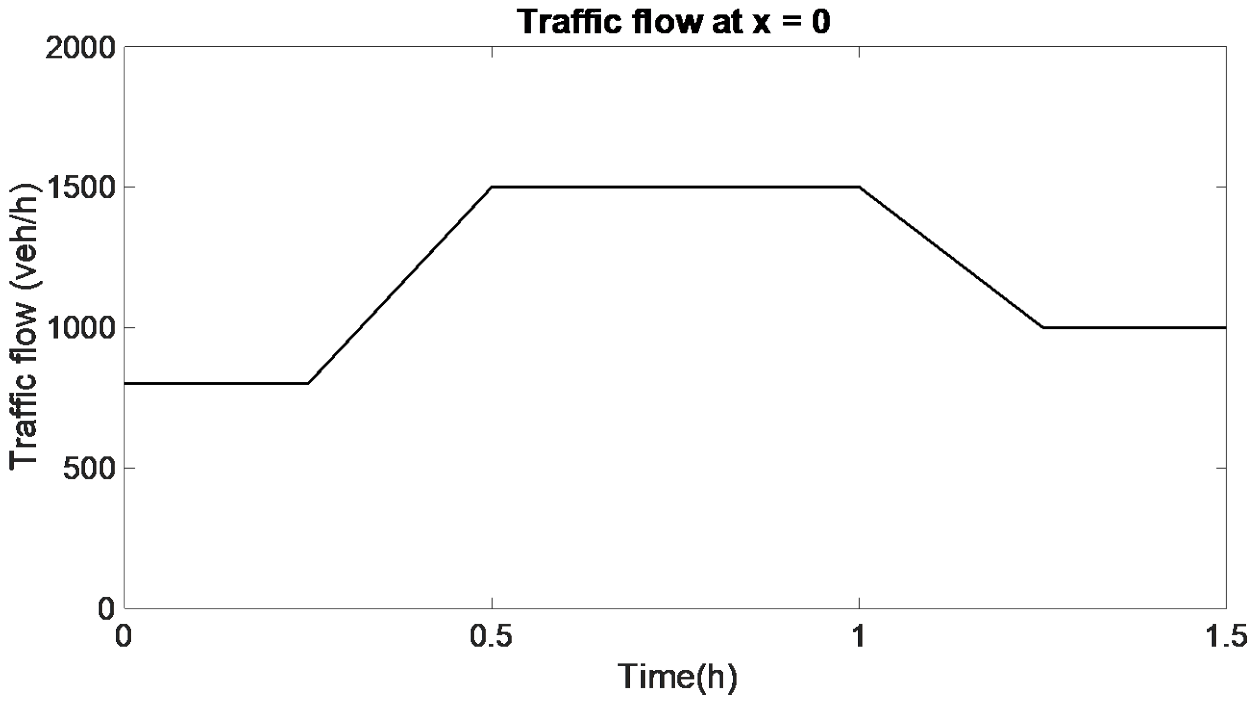

FIGURE 2. Traffic flow at the left boundary.

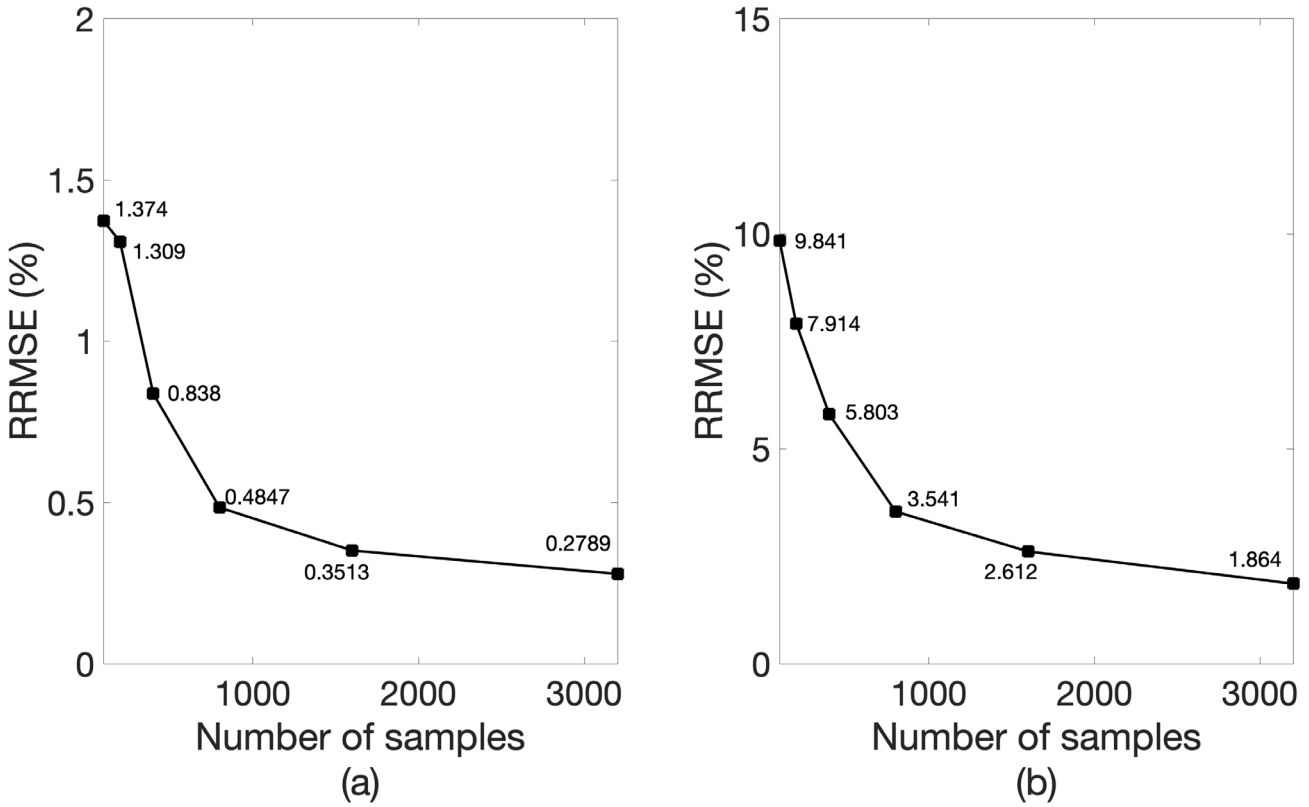

FIGURE 3. RRMSE of different numbers of samples: (a) MEAN and (b) SDEV.

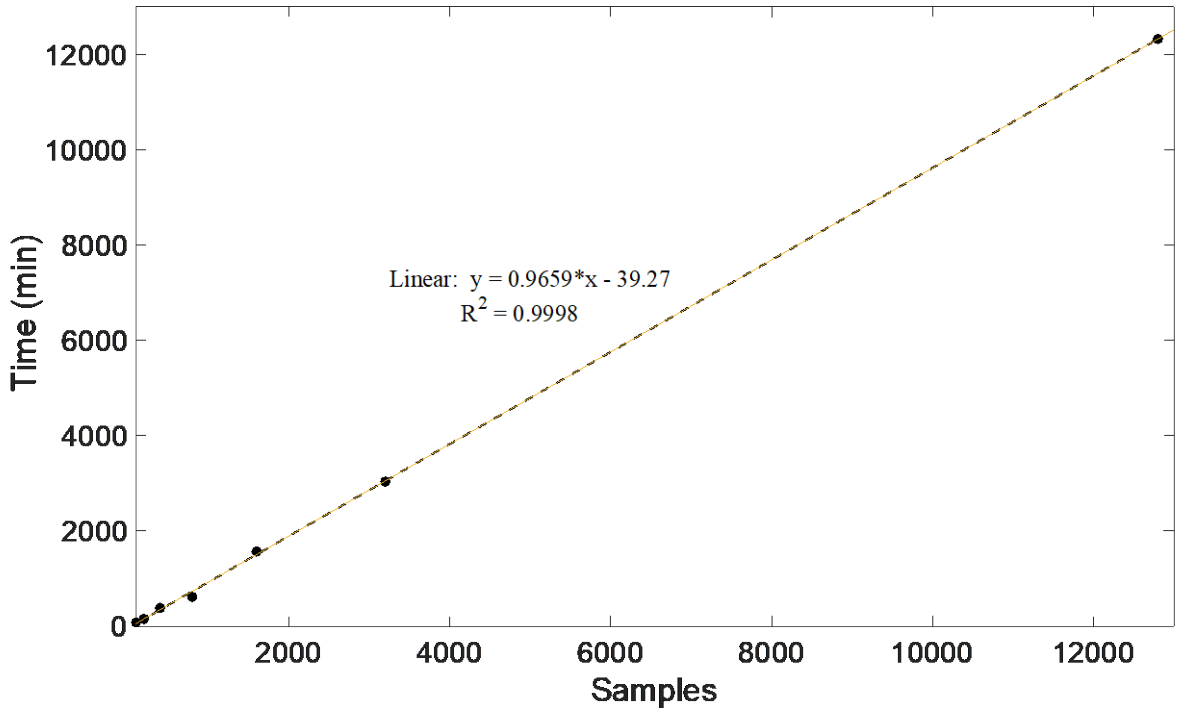

FIGURE 4. Computation time of the MC method.

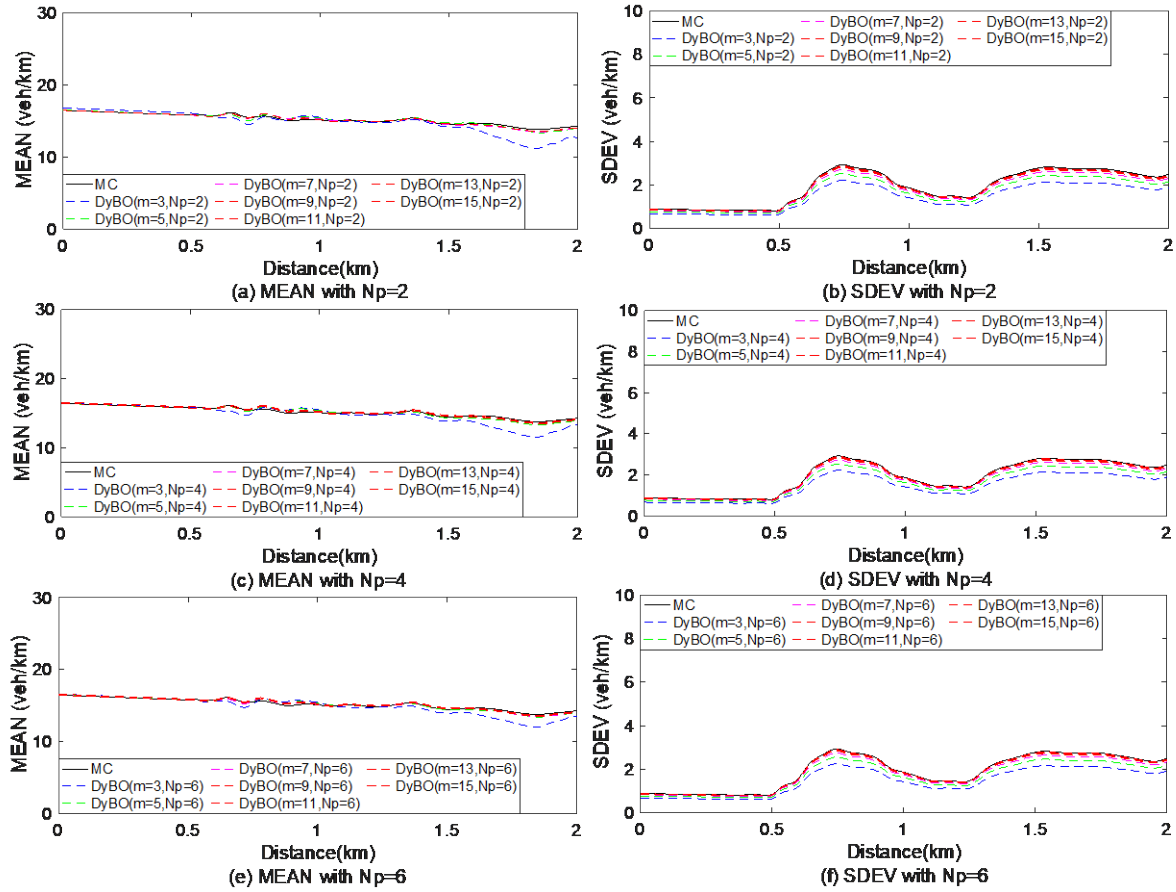

FIGURE 5. Density patterns at t = 0.3 h.

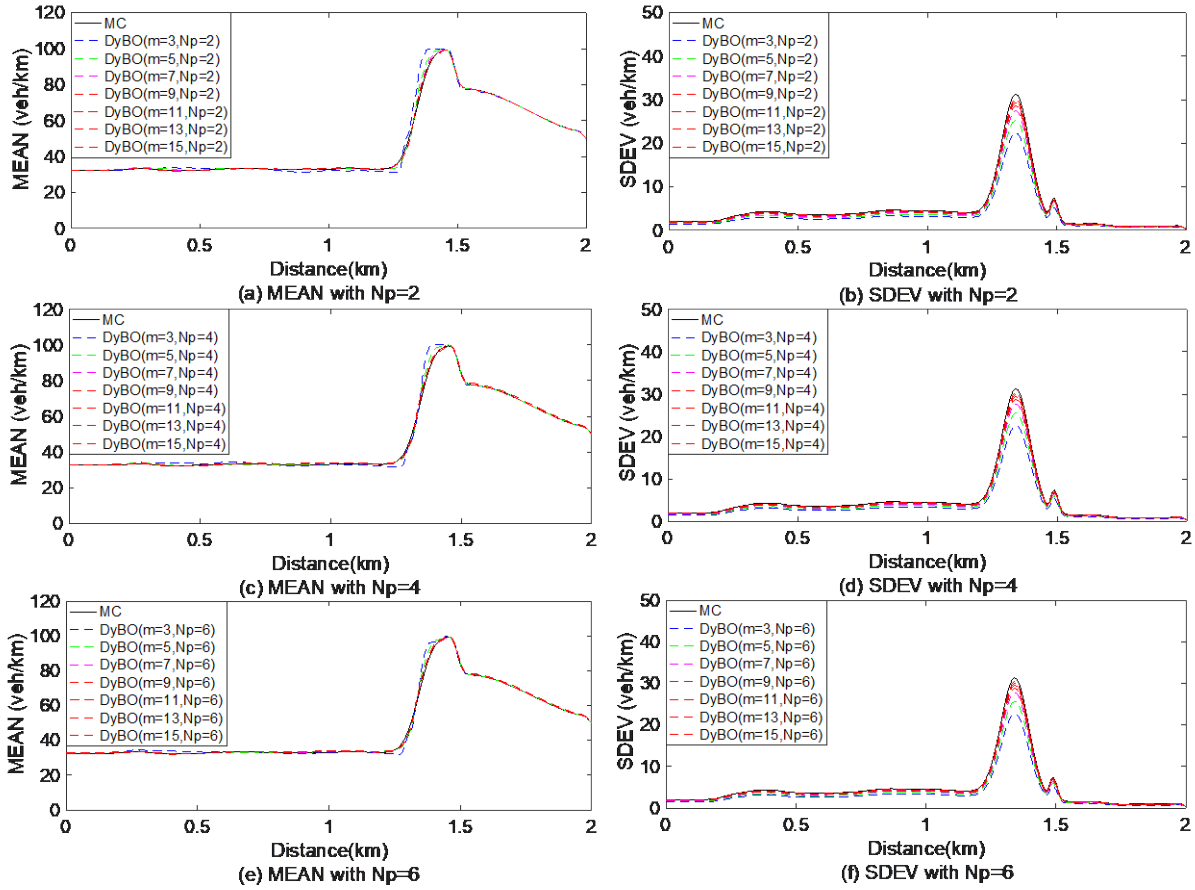

FIGURE 6. Density patterns at t = 0.78 h.

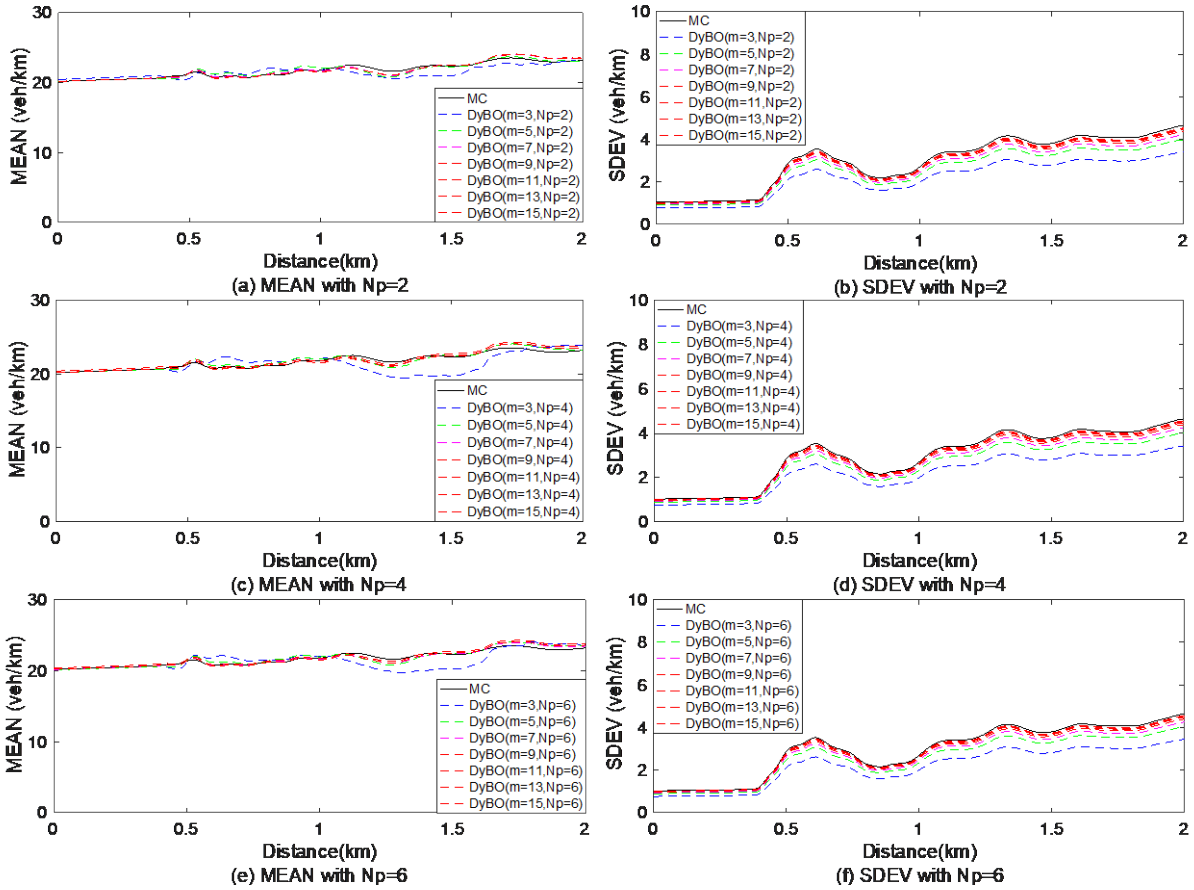

FIGURE 7. Density patterns at t = 1.2 h.

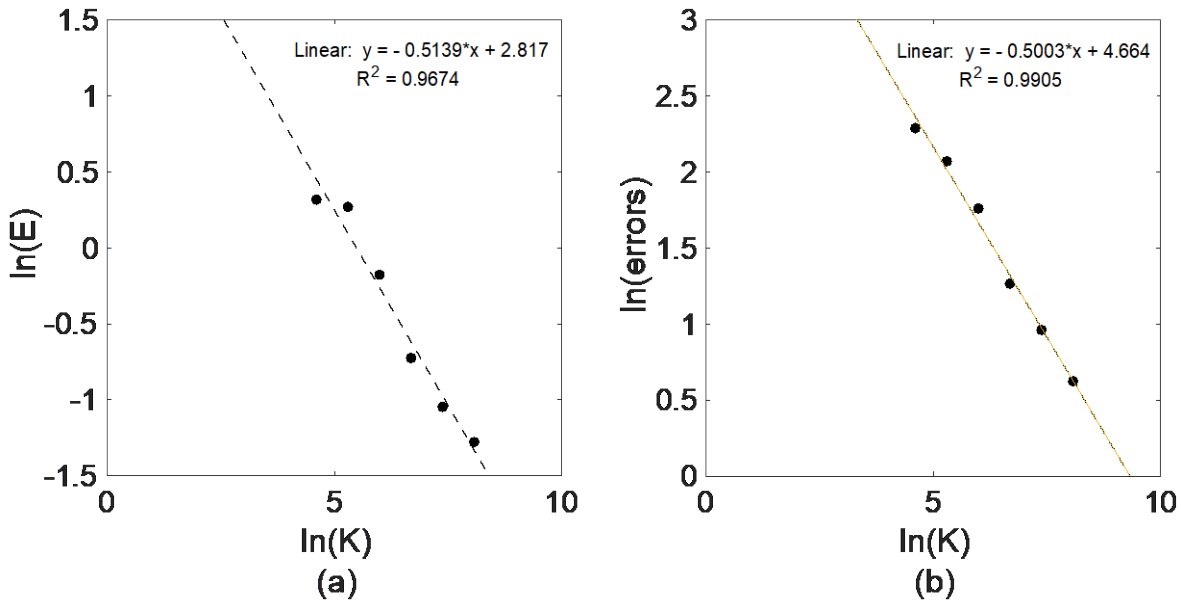

FIGURE 8. Relationship between the number of samples and errors of the MC method: (a) MEAN and (b) SDEV.

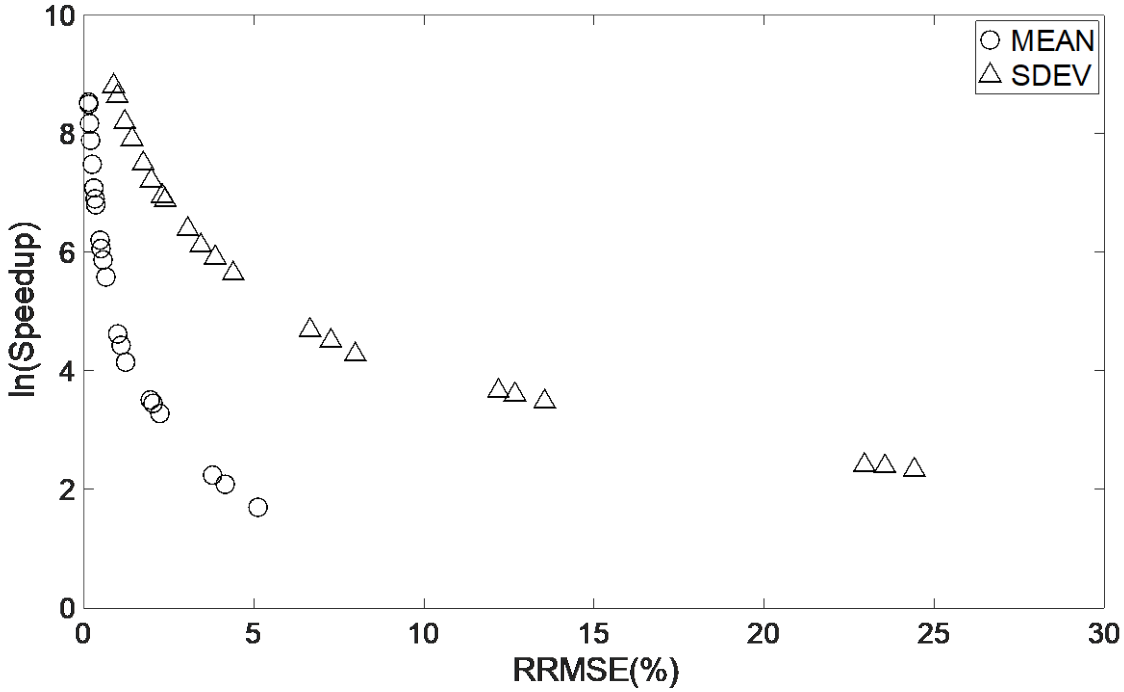

FIGURE 9. Relationship between speedup and RRMSE.